Cell, Vol. 81, 811–823, June 2, 1995, Copyright © 1995 by Cell Press

Targeted Disruption of the Huntington's Disease Gene Results in Embryonic Lethality and Behavioral and Morphological Changes in Heterozygotes

Jamal Nasir,* Stan B. Floresco,† John R. O'Kusky,‡ Virginia M. Diewert,§ Joy M. Richman,§ Jutta Zeisler,*‖ Anita Borowski,# Jamey D. Marth,# Anthony G. Phillips,† and Michael R. Hayden*‖

*Department of Medical Genetics
†Department of Psychology
‡Department of Pathology and Laboratory Medicine
§Department of Clinical Dental Sciences
#Biomedical Research Centre
‖Centre for Molecular Medicine and Therapeutics
University of British Columbia
Vancouver, British Columbia V6T 1Z4
Canada

Summary

Huntington's disease (HD) is an incurable neuropsychiatric disease associated with CAG repeat expansion within a widely expressed gene that causes selective neuronal death. To understand its normal function, we have created a targeted disruption in exon 5 of *Hdh* (*Hdh*^{ex5}), the murine homolog of the HD gene. Homozygotes die before embryonic day 8.5, initiate gastrulation, but do not proceed to the formation of somites or to organogenesis. Mice heterozygous for the *Hdh*^{ex5} mutation display increased motor activity and cognitive deficits. Neuropathological assessment of two heterozygous mice shows significant neuronal loss in the subthalamic nucleus. These studies show that the HD gene is essential for postimplantation development and that it may play an important role in normal functioning of the basal ganglia.

Introduction

Huntington's disease (HD) is a devastating neurological disease associated with chorea, cognitive deficit, psychiatric disturbances, and inexorable progression to death, typically 10–15 years after onset. It usually manifests in midlife, affects approximately 1 in 10,000 individuals (Hayden, 1981), and results in selective neuronal loss that is most prominent in the striatum and basal ganglia (Vonsattel et al., 1985).

The HD gene (*IT15*) (Huntington's Disease Collaborative Research Group, 1993) is ubiquitously expressed (Strong et al., 1993; Li et al., 1993) and conserved across a wide range of species (Lin et al., 1994). Structural analysis of its promoter region is consistent with its being a housekeeping gene (Lin et al., 1995). *IT15* encompasses 67 exons, spans over 200 kb (Ambrose et al., 1994), and is associated with two transcripts of 10.3 kb and 13.6 kb, differing with respect to their 3′ untranslated regions (Lin et al., 1993). In addition, *IT15* encompasses a highly polymorphic CAG repeat that varies in number from eight to 35 in normal individuals (Kremer et al., 1994). CAG expansion beyond 36 CAG repeats is seen in persons with HD. A similar mutational mechanism is associated with five other neurodegenerative diseases that are also associated with expansions of CAG repeats within their coding regions (Willems, 1994). Lack of homology to other genes or to any obvious functional domains has meant that the function of these genes has hitherto remained a mystery. In particular, the question of how these widely expressed genes cause selective neuronal death remains unanswered.

We have previously mapped (Nasir et al., 1994), cloned, and sequenced (Lin et al., 1994) *Hdh*, the murine homolog of the HD gene, which shares a high degree of homology with its human homolog but differs with respect to length of its CAG repeat. In mouse there are only seven CAG repeats that are interrupted at the third triplet with CAA.

To gain further insights into the physiological role of the HD gene during growth and development, we generated mice with a targeted disruption of the HD gene. We have created null mutants by inserting the neomycin (*neo*) gene cassette into exon 5 of *Hdh* (*Hdh*^{ex5}). We have demonstrated that mice derived from three independently targeted embryonic stem (ES) cell lines do not survive to term and suffer early postimplantation embryonic lethality. Heterozygotes for this mutation have increased motor activity and cognitive deficits associated with neuronal loss in the subthalamic nucleus of the basal ganglia. These data show that the HD gene is essential for normal embryonic development and suggest a role for this gene in normal development of the basal ganglia.

Results

Targeted Disruption of the *Hdh* Gene

A genomic library from the 129/Sv mouse strain was screened with a murine cDNA clone encompassing exon 5 (Lin et al., 1994). Several clones were recovered and restriction mapped in detail, and exon–intron boundaries were sequenced (Lin et al., 1995).

To create a disruption in exon 5 of the *Hdh* gene (*Hdh*^{ex5}), we generated the targeting construct pHdhNeo6 (Figure 1A) by deleting approximately half of exon 5 plus intron 4 sequences and replacing them with a *PGKneobpA* cassette. Disruption of murine exon 5 results in stop codons in all reading frames.

Screening for Homologous Recombination

A total of 360 G418-resistant colonies were picked and screened by polymerase chain reaction (PCR) using a *neo*-specific primer (*P7*) and a primer (*P6*) flanking the integration site (Figure 1A). The expected size fragment (1.3 kb) was detected in five pools (Figure 1B). Individual clones corresponding to each positive pool were separately screened by PCR. Six clones were identified, indicating a targeting frequency of 1 in 60 G418-resistant clones (6 of 360).

Three independently targeted ES cell lines were estab-

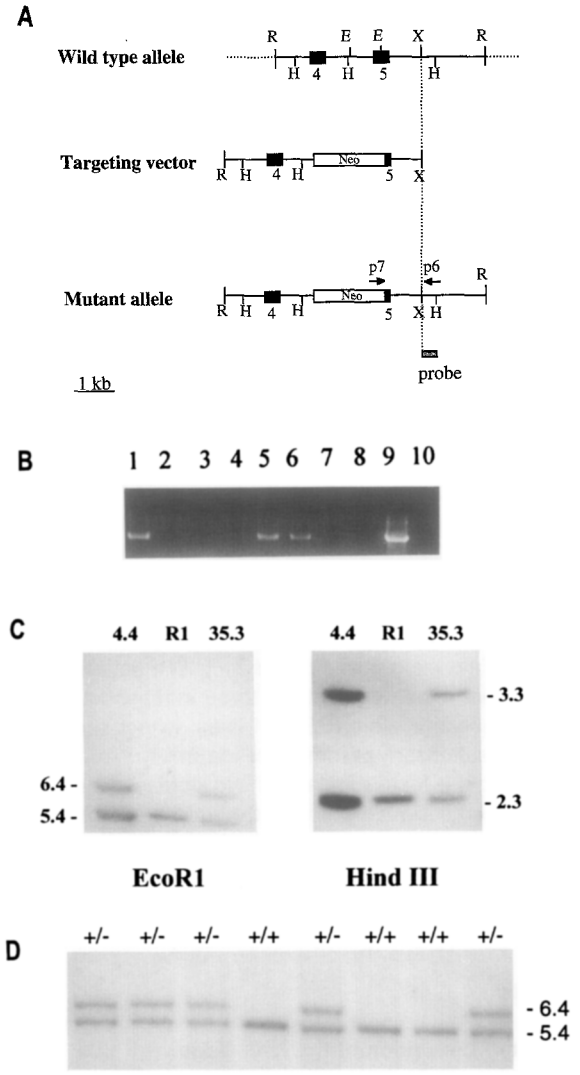

Figure 1. Targeted Disruption of the *Hdh* Gene

(A) The targeting vector and its relationship to the wild-type allele are depicted. The relative positions of exons 4 and 5 are as indicated. The targeting vector was generated by replacing a 600 bp EspI fragment encompassing a portion of exon 5 plus part of intron 4 with a *PGKneobpa* cassette (see Experimental Procedures). The locations of the PCR primers (*P6* and *P7*) used to screen for homologous recombination and the genomic probe used to confirm this are also given. Note that the insertion of the *neo* cassette at exon 5 leads to an increase in size of the HindIII and EcoRI fragments encompassing this genomic region. Abbreviations: R, EcoRI; H, HindIII; X, XbaI; E, EspI.

(B) DNAs derived from clonal ES cell lines were screened by PCR using primers *P6* and *P7*. The expected 1.3 kb PCR product was detected in lanes corresponding to ES clones 4.4 (lane 1), 35.3 (lane 5), and 35.8 (lane 6). This product was detected in the positive control (lane 9), but not in the two negative controls containing mouse genomic DNA (lane 8) and no DNA (lane 10).

(C) EcoRI and HindIII digests of clones 4.4 and 35.3 hybridized with a genomic probe (see [A]). In EcoRI digests, two fragments were detected corresponding to the wild-type (5.4 kb) and mutant (6.4 kb) alleles. Similarly, with HindIII digests, both the wild-type (2.3 kb) and mutant (3.3 kb) alleles were detected. As expected, for the nontransfected cell line (R1), only the wild-type allele was identified with EcoRI and HindIII digests.

(D) Agouti offspring of chimeric mice were assessed for germline transmission by digesting their DNAs with EcoRI, followed by hybridization with a genomic probe (see [A]). Thus, wild-type (+/+) and heterozygous (+/−) mice were identified.

Table 1. Generation of Chimeric Mice and Germline Transmission of Mutant Allele

Clone	Chimera	Agouti (%)	Sex	Agouti Offspring	Germline Transmission
4.4	88	70	M	23 of 32	Yes
	93	50	F	—	—
	97-1	95	M	23 of 23	Yes
	97-2	90	M	24 of 24	Yes
35.3	94-1	>95	M	23 of 23	Yes
	94-2	>95	M	22 of 22	Yes
	94-3	>95	M	14 of 14	Yes
	94-4	80	F	14 of 14	Yes
	94-5	40	M	0 of 18	No
	100	70	F	0 of 10	No
35.8	109-1	90	M	—	—
	109-2	80	M	3 of 3	Yes
	109-3	60	M	0 of 21	No
	109-4	10	F	—	—

Three independently derived correctly targeted ES clones were injected into blastocyst stage embryos (see Experimental Procedures) to generate chimeric animals. The majority of the chimeric animals had a very high ES cell contribution as determined by the extent of agouti in their coat color. Generally, only males were selected for further breeding to identify the germline-transmitting animals.

lished, and the targeting event was confirmed in each by Southern blot analysis. For each cell line, EcoRI and HindIII digests were performed followed by hybridization using a 600 bp genomic probe derived from sequences outside the region of homologous recombination (Figure 1A). The predicted sizes for the digested fragments associated with the wild-type allele are 5.4 kb and 2.3 kb, respectively. The insertion in exon 5 results in a corresponding increase in fragment lengths from 5.4 kb to 6.4 kb for EcoRI and from 2.3 kb to 3.3 kb for HindIII (see Figure 1C). In the nontransfected control, R1, only the wild-type allele was detected. In the targeted cell lines 4.4, 35.3, and 35.8 (data not shown), both wild-type and mutant fragments were observed at equivalent intensities (Figure 1C).

Generation of Chimeric Mice

ES cells from each cell line (4.4, 35.3, and 35.8) carrying the targeted *Hdh* mutation were injected into C57BL/6J blastocysts and implanted into pseudopregnant foster mothers. Male chimeras were bred to either C57BL/6J or chimeric females. All three clones generated high levels of chimerism (typically at least 70%), and germline transmission was achieved for each clone (Table 1). Approximately half the agouti pups were heterozygous for the mutation (+/−) and half were wild-type (+/+) (Figure 1D).

Reverse Transcription-PCR Analysis of Heterozygous Mice

To confirm that the targeted mutation in exon 5 results in a null allele, we performed reverse transcription PCR (RT-PCR) on RNA from brains of heterozygous mice and a wild-type mouse. RNA from two female heterozygous mice originating from different ES cell lines (4.4 and 35.3) was reverse transcribed using a gene-specific primer (*P16*) and random hexamers.

The RT product was used as a template for PCR amplifi-

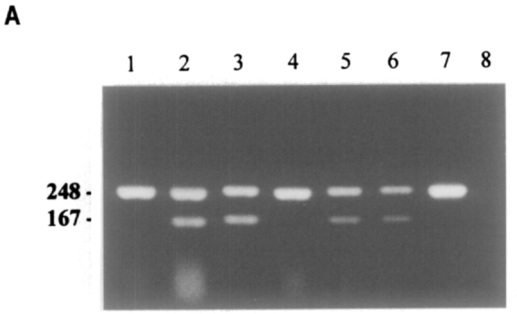

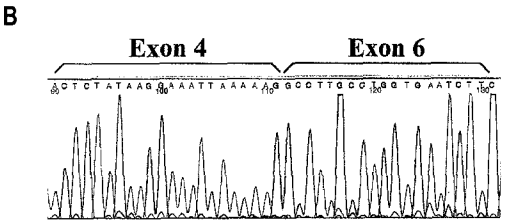

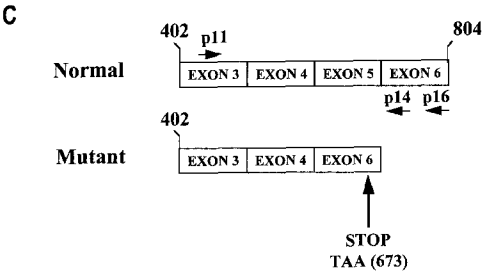

Figure 2. Targeted Disruption Results in a Premature Stop Codon at Exon 6

(A) RT–PCR analysis of heterozygous mice. RNA was extracted from two adult heterozygous (+/–) mice derived from ES cell lines 4.4 (lanes 2 and 5) and 35.3 (lanes 3 and 6). As a control, RNA from a wild-type mouse (+/+) (lanes 1 and 4) was used. Lanes 7 and 8 are (+/–) controls. The RT–PCR was carried out using a gene-specific primer (lanes 1–3) and random hexamers (lanes 4–6). The RT product was amplified using primers derived from exons 4 and 6 (see Experimental Procedures). The expected 248 bp product is seen in all lanes except lane 8, which has no DNA. However, in lanes 2, 3, 5, and 6, corresponding to RT products derived from the heterozygous mice, a short PCR product (167 bp) is also seen.

(B) Sequencing of the shorter (167 bp) RT–PCR product in heterozygous mice confirms that exon 5 is skipped in the mutant allele.

(C) In the wild-type allele, all exons are correctly spliced, whereas in the mutant allele, exon 5 is skipped, leading to a premature termination of the translated protein in exon 6. The RNA was reverse transcribed with primer *P16* and PCR amplified with primers *P11* and *P14* (see Experimental Procedures).

cation using primers from exon 3 (*P11*) and exon 6 (*P14*). The expected 248 bp product was generated from RNA of both the heterozygous mice and the control mouse (Figure 2A). In the heterozygous mice, a shorter product (167 bp) was generated as predicted, presumably due to the skipping of exon 5 (see Figure 2). To confirm this, this product was subcloned and sequenced (Figure 2B), revealing that the mutation leads to skipping of exon 5 and a frameshift resulting in a stop codon immediately downstream of the targeting event at nucleotide 673 that results in a severely truncated protein of approximately 20 kDa (Figure 2C).

Table 2. Genotyping of Liveborn Offspring

Source (Cell Line)	(+/+)	(+/–)	(–/–)
4.4	46	80	0
35.3	31	59	0
35.8	4	5	0
Total	81	144	0

Heterozygous mice for each of three ES cell lines (4.4, 35.3, and 35.8) were intercrossed, and the resulting liveborn offspring were genotyped. $\chi^2 = 73.125$; df = 2; $p < 10^{-6}$.

Western blot analysis of brains from heterozygous mice using an antibody (AP78) directed against the N-terminus of the protein (Sharp et al., 1995) revealed an approximately 340 kDa band indicative of the product from the normal allele, and a smaller protein of approximately 20 kDa that could represent the truncated gene product.

Disruption of *Hdh* Mutation Results in Early Embryonic Lethality

Mice heterozygous for the targeted mutation were intercrossed, but no live homozygous *Hdh*^{ex5} mice were produced among 225 newborns ($p < 10^{-6}$) (Table 2) derived from all three independently targeted ES cell clones. The number of heterozygotes to wild-type mice were present in the ratio of approximately 2:1, which allowed us to conclude that the *Hdh*^{ex5} homozygotes die in utero.

To determine the timing of the *Hdh*^{ex5} lethality, embryos were analyzed at different stages during gestation. From embryonic day 7.5 (E7.5) to E12.5, 173 decidua analyzed contained morphologically normal embryos (Table 3), whereas the remaining 51 contained nearly or completely resorbed embryos, 35 of which were recovered for genotyping (Table 4). The embryos were genotyped by Southern blot or PCR analysis (Figures 3A and 3B). Normal embryos were in the expected ratios for genotypes (+/+) or (+/–), but only four (2%) phenotypically normal embryos (two at E7.5) had the (–/–) genotype (Table 3). The majority (80%) of resorbed embryos were homozygous for the *Hdh*^{ex5} mutation (Table 4). These data indicate that loss of function of the endogenous *Hdh* gene results in embryonic lethality during early postimplantation development.

Histological Analysis of Embryos

From E7.5 to E9.5, a high frequency of resorption in the litters of heterozygote crosses was observed (40 of 187 or 21.3%). At E8.5, the ratio of (–/–) versus (+/+) or (+/–) resorbed embryos increased, indicating that more *Hdh*^{ex5} homozygotes were dying.

Sections from 67 embryos produced by heterozygous intercrosses were examined. Litters ranged in age from 7 to 8.5 days gestation, during which time the major events of gastrulation have occurred: elongation of the primitive

Table 3. Genotyping of Phenotypically Normal Embryos at Different Stages of Gestation

Day of Gestation	(+/+)	(+/−)	(−/−)
7.5	23	24	2
8.5	16	46	2
9.5	9	16	0
10.5	8	12	0
11.5	2	6	0
12.5	1	6	0
Total	59	110	4

Timed matings were set up between heterozygous animals for each clone, and both normal and resorbed embryos were collected at different stages of gestation (E7.5–E12.5). $\chi^2 = 47.5818$; df = 2; $p < 10^{-6}$.

streak, formation of mesoderm, formation of headfolds, and the formation of somites and branchial arches. The abnormal embryos (19 of 67 or 28.36%) could be distinguished by their immaturity compared with normal littermates (compare Figure 4A with Figure 4B; compare Figure 4C with Figure 4D). The disparity in development was most evident in the older litters, collected at 7.75 and 8.5 days gestation.

The normal embryos exhibited well-developed headfolds and epithelial-stage somites (Figures 4F and 4H; data not shown), whereas the abnormal littermates only reached late primitive streak stage (Figures 4G and 4I). In the developmentally delayed embryos, there was no indication that a neural plate had formed (compare Figures 4C and 4D), although mesoderm had accumulated between the ectoderm and endoderm. The extraembryonic membranes were present in the abnormal embryos in the same arrangement as in normal embryos (Figure 4E; data not shown). However, the size of the membranes was reduced, and a connection between the allantois and the placenta was not achieved. The phenotype of abnormal embryos closely matches that of the dissected, genotyped embryos (compare Figures 4B and 4D with Figures 4I and 4J). Null mutants deteriorated rapidly after 8.5 days, and little structure remained by 10.5 days gestation (Figure 4K).

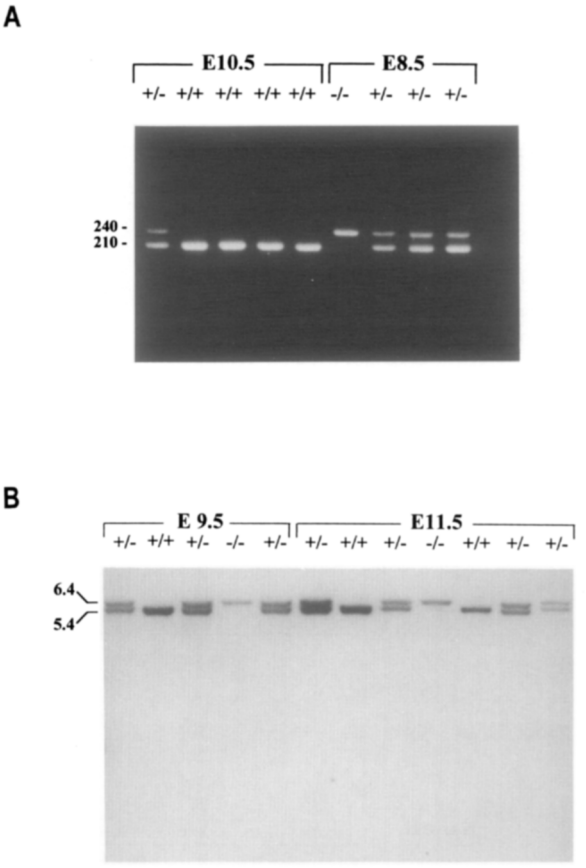

Figure 3. Genotype Analysis of Embryos at Different Stages of Gestation

(A) Embryos were incubated overnight in a lysis buffer including proteinase K and were analyzed by PCR with primers *P8*, *P9*, and *P586* (see Experimental Procedures). The PCR products were run on 2% agarose gels to resolve the wild-type (210 bp) and mutant (240 bp) alleles.

(B) For Southern blot analysis, DNA was isolated as described elsewhere (Hogan et al., 1986). The DNA was digested with EcoRI, blotted, and hybridized with a genomic probe (Figure 1A). The wild-type and mutant alleles are associated with fragment sizes of 5.4 kb and 6.4 kb, respectively.

Behavioral Assessment

Seven mice heterozygous for the *Hdh*^{ex5} mutation and seven wild-type mice (+/+) from related litters were assessed. All mice were 4-month-old males. Mutant mice ate and drank normally, were indistinguishable from controls with respect to body weight, posture, locomotion, rearing, and grooming, and did not display any signs of ataxia. Mutant mice were distinctly more reactive to handling. For all tests, the experimenter was blind to the genetic status of the animals.

Table 4. Genotyping of Resorbed Embryos at Different Stages of Gestation

Day of Gestation	(+/+)	(+/−)	(−/−)
7.5	2	1	2
8.5	1	1	12
9.5	—	1	9
10.5	1	—	2
11.5	—	—	2
12.5	—	—	1
Total	4	3	28

Timed matings were set up between heterozygous animals for each clone, and both normal and resorbed embryos were collected at different stages of gestation (E7.5–E12.5). $\chi^2 = 70.7321$; df = 2; $p < 10^{-6}$.

Motor Activity Test

This test assessed spontaneous motor activity in a horizontal plane, as measured by overall level of activity and the habituation to a novel stimulus during each separate 2 hr phase of the test. The mutant mice were significantly more active than controls ($p < 0.01$) throughout both phases, with no overlap between the groups (in the light-phase mutant, 2162 ± 163; control, 1557 ± 163; $p < 0.05$; in the dark-phase mutant, 1383 ± 133; control, 714 ± 133; $p < 0.005$) (Figure 5A). Activity scores of both

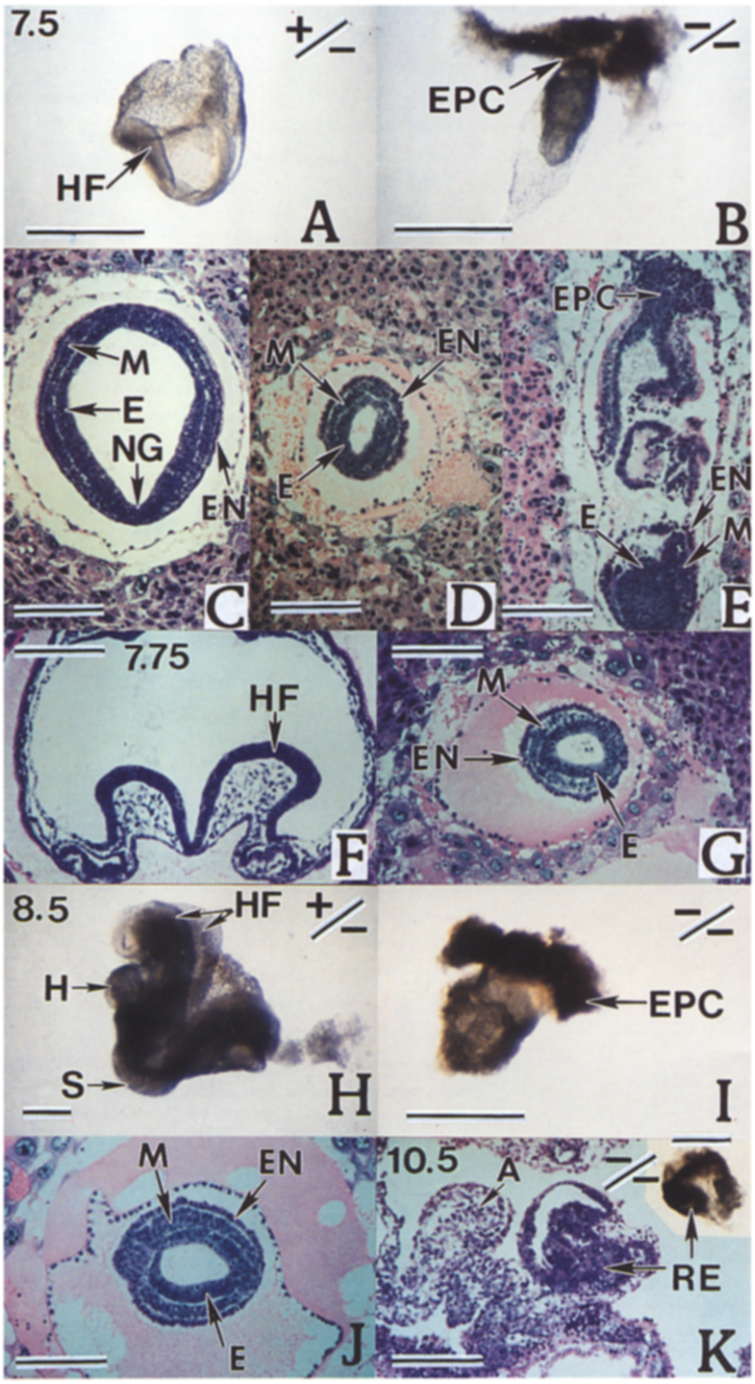

Figure 4. Mouse Embryos Produced by Heterozygous Intercrosses

Embryos in (A), (B), (H), (I), and (K) were genotyped using PCR. The scale bar for whole embryos is 500 μm; the scale bar for sectioned embryos is 250 μm. Abbreviations: A, allantois; E, embryonic ectoderm; EPC, ectoplacental cone; EN, embryonic endoderm; HF, headfold; H, heart; M, mesoderm; NG, neural groove; RE, resorbing embryo; S, somite.

(A) Heterozygous embryo dissected out of the decidua. Headfolds have begun to form at the anterior end of the embryo.

(B) Homozygous littermate of the embryo in (A). The embryo is very small and underdeveloped.

(C) Transverse section of an E7.5 normal embryo. The neural groove has begun to form in this early neurula-stage embryo.

(D) Transverse section of an abnormal (E7.5) embryo. Mesoderm has formed around the embryonic ectoderm. The size of the embryo is considerably smaller than the normal embryo shown in (C).

(E) Parasagittal section of an abnormal (E7.5) embryo shows that a small amount of mesoderm has formed in the embryo. However, extraembryonic membranes are fragmented, and the process of resorption may be beginning.

(F) Transverse section through the headfold region of an E7.75 normal embryo.

(G) Transverse section through an abnormal (E7.75) embryo shows that mesoderm has formed. However, the ectoderm is not thickened, as occurs normally at the onset of neurulation.

(H) Heterozygous embryo (E8.5) dissected out of decidua. Prominent headfolds, heart, and somites are visible.

(I) Homozygous littermate to the embryo in (H). The size of the embryo is considerably smaller than its normal littermate.

(J) Transverse section of an abnormal E8.5 embryo in which development is similar to that of the embryo in (I). The embryo is very small and looks similar to abnormal embryos observed at 7.5 and 7.75 days gestation. Mesoderm has formed, but neurulation has not begun.

(K) Section through an E10.5 (−/−) resorbing embryo showing complete disorganization of embryonic tissue layers and membranes. Inset shows appearance of small undeveloped embryo and membranes prior to sectioning.

groups declined significantly across successive 10 min time bins ($p < 0.01$).

T Maze Alternation Test

This test allows general assessment of simple discrimination learning and short-term memory. Both groups learned this task at the same rate ($F[2,20] = 12.349$; $p < 0.001$) and reached asymptotic performance of 80% or greater correct responses by training day 3. They also did not differ in mean latency to reach the food cup after release (*Hdh*^{ex5} mice, 35.6 ± 2.9 s; control mice, 39.1 ± 7.1 s), which provides confirmation that mutant mice did not have impairments in locomotion and that motivation was normal. One animal in both the mutant and control groups did not eat Froot Loops during any trial on the T maze, and therefore their data were not analyzed.

Radial-Arm Maze Test

This provides a direct test of working memory. Control animals quickly learn not to revisit arms explored previously within a trial and thus acquire the four pieces of food with minimum effort. Data were excluded from the

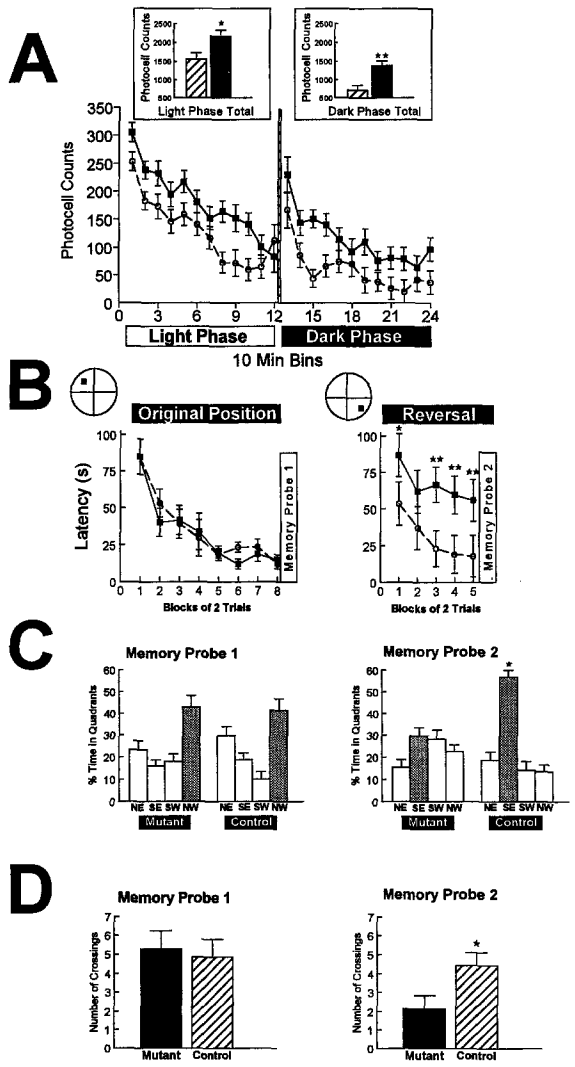

Figure 5. Behavioral Studies in Mice Heterozygous for the *Hdh*^{ex5} Mutation

(A) Locomotion activity (mean ± SEM) as measured by photocell beam breaks for *Hdh*^{ex5} knockout mice (closed squares) and controls (open circles) during the light and dark phases of the 4 hr testing session. *Hdh*^{ex5} mice were more active relative to controls over the entire session ($F[1,12] = 10.687$; $p < 0.01$). Mice in both conditions showed habituation over the session ($F[11,132] = 5.305$; $p < 0.001$). There was no significant interaction. Insert graphs show total photocell counts (mean ± SEM) for *Hdh*^{ex5} mice (closed bar) and control mice (hatched bar) for the light phase and dark phase of the locomotion testing session. *Hdh*^{ex5} mice were more active during both the light phase ($F[1,12] = 6.841$; $p < 0.05$) and dark phase ($F[1,12] = 12.509$; $p < 0.005$) than control mice (*, $p < 0.05$; **, $p < 0.01$).

(B) Morris water maze testing. Latencies to find the hidden platform (mean ± SEM) for *Hdh*^{ex5} mice (closed squares) and controls (open circles) with the platform in the original position (left) and during the reversal (right) when the platform was moved to the opposite quadrant. A highly significant effect of trial was observed ($F[12,144] = 9.639$; $p < 0.001$), indicating that both groups of mice showed improvements in performance over trials. Furthermore, a significant interaction was observed ($F[12,144] = 2.366$; $p < 0.01$). *Hdh*^{ex5} mice were significantly slower to find the hidden platform during blocks 1, 3, 4, and 5 of the reversal trial (*, $p < 0.05$; **, $p < 0.01$).

(C) Percentage of time spent in the four quadrants of the water maze during memory probe trial 1 (left) and trial 2 (right), given after the initial acquisition and reversal phases, respectively. Analysis of the memory trial showed that mice in both groups spent more time in the quadrant where the platform had recently been located (stippled bar) relative to the other three quadrants (open bars) ($F[3,36] = 14.695$; $p < 0.001$; Tukey's post hoc, $p < 0.01$). During memory probe trial 2, a significant interaction was observed ($F[3,36] = 8.194$; $p < 0.01$). Control mice spent more time in the quadrant where the platform had recently been located (stippled bar) relative to the other three quadrants (open bars) ($p < 0.01$), while *Hdh*^{ex5} mice distributed their swim time equally across all four quadrants (*, $p < 0.05$).

(D) Number of crosses of the location of the platform (mean ± SEM) for *Hdh*^{ex5} knockout mice (closed bar) and controls (hatched bar) during memory probe trial 1 (left) and memory probe trial 2 (right). No differences between groups were observed during memory probe trial 1. However, control mice crossed the location of the platform significantly more often than *Hdh*^{ex5} mice during memory probe trial 2 following reversal training ($F[1,12] = 5.408$; $p < 0.05$). Asterisk denotes significance at $p < 0.05$.

same two mice that once again did not eat during this test. Although the performance of the mutant mice, as measured by reentry errors, was highly variable, the mutant group did not differ from controls, and both groups made fewer errors as the experiment proceeded ($F[16,60] = 2.757$; $p < 0.05$). *Hdh*^{ex5} mice made 2.0 ± 0.05 revisit errors on training day 7 compared with 1.0 ± 0.47 errors by the control group.

Morris Water Maze Task

The Morris water maze task (Morris, 1981) has been used routinely to study the ability of rodents to acquire spatial information. Measures of path length and latency to reach a submerged platform were grouped across acquisition and reversal phases. Both groups of mice showed improvement over 16 trials. Analyses of the latency data confirmed that *Hdh*^{ex5} mice had acquired the necessary spatial information to locate the hidden platform efficiently (see Figure 5B). A separate analysis of the path length measurements showed no effect of genotype and a significant effect of trial ($F[12,144] = 17.31$; $p = 0.001$) with no significant interaction. Two mutant mice remained motionless for 20–30 s periods during several of the reversal trials, which may have enhanced the latency scores without increasing path length.

Data from the memory probe trial demonstrated appropriate memory for the location of the platform site by both *Hdh*^{ex5} and control mice, reflected by the greater percentage of time spent by both groups in the northwest quadrant of the pool ($p < 0.001$) (see Figure 5C), where the platform had previously been located. Both *Hdh*^{ex5} and control mice made a comparable number of crosses over the platform site (Figure 5D).

Deficits were, however, observed when mutants were required to reverse their spatial response by swimming to the hidden platform in a new location (Figure 5B). Latency data from the *Hdh*^{ex5} group were significantly greater than in the control group on the first, third, fourth, and fifth blocks of trials ($p < 0.01$). A second memory probe trial conducted immediately after the tenth reversal trial confirmed the impairment (Figure 5C). Control mice again spent a significantly greater percentage of the trial swimming in the quadrant in which the platform had been relocated ($p < 0.01$). By contrast, *Hdh*^{ex5} mice distributed their swimming time equally across all four quadrants. This difference was highlighted by the finding that control mice crossed the new platform site in the southeast quadrant

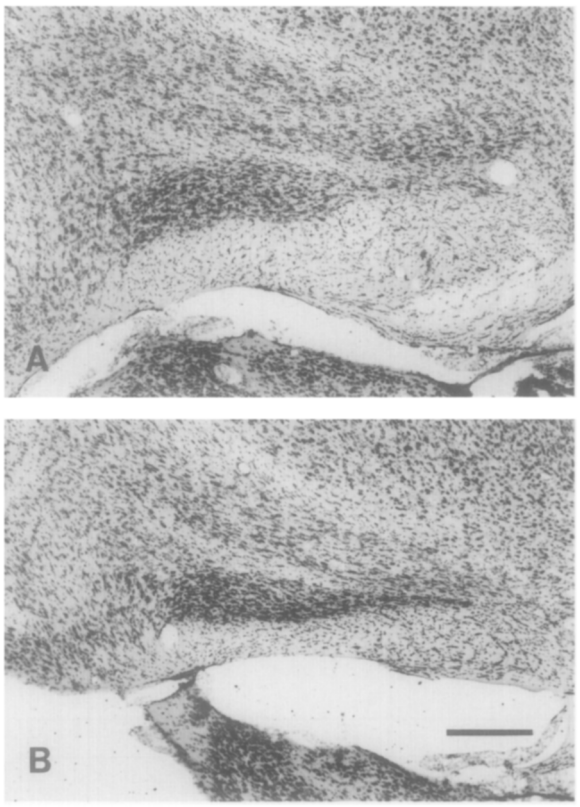

Figure 6. Nissl Sections through the Subthalamic Nucleus

The subthalamic nucleus was easily recognized in both wild-type controls (A) and heterozygous mice (B) as a small elongated nucleus containing densely packed, darkly stained neurons located between the zona incerta dorsally and the cerebral peduncle ventrally. The nucleus is ovoid medially (left) with a tail extending laterally (right). Note the decreased size of the nucleus in (B), which is most evident in the middle third. Scale bar, 300 μm.

more than twice as frequently as did the mutant mice ($p < 0.05$). Normal acquisition and memory of spatial information coupled with the marked impairment seen in the reversal trials suggest that *Hdh*^{ex5} mice have cognitive deficits associated with acquiring or using new information in the face of existing information.

Histology and Morphometry of Brains of Heterozygotes

Two heterozygous mice with the most severe performance deficits were sacrificed for neuropathological examination. The morphology of the central nervous system in the heterozygous mice appeared relatively normal, with no signs of gross malformations or obvious developmental abnormalities. Examining the serial Nissl sections revealed no signs of neuronal necrosis, gliosis, or inflammation. In the heterozygous mice, there appeared to be a decrease in the size of the subthalamic nucleus (Figure 6). There were no obvious differences in the morphology of the caudate/putamen (Figure 7), although there appeared to be a decrease in the number of neurons in the globus pallidus (see Table 5). The cerebral cortex and corpus callosum appeared normal.

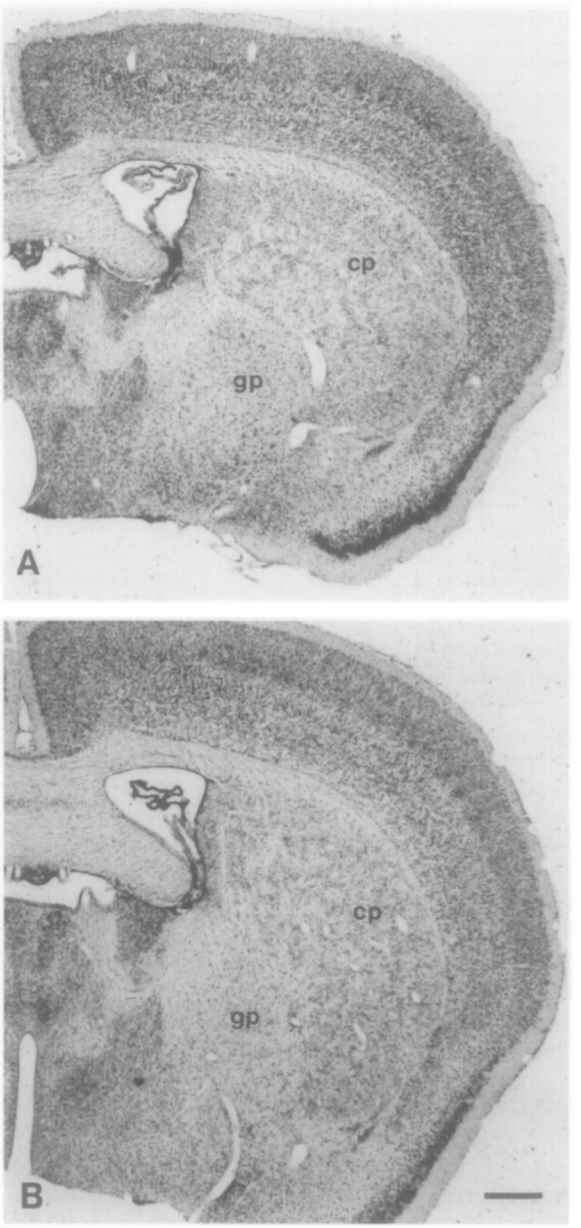

Figure 7. Nissl Sections through the Striatum

Frontal sections through the caudate/putamen (cp) and globus pallidus (gp) of wild-type control (A) and heterozygous mice (B) are shown. Scale bar, 500 μm.

There were no differences in mean brain weight, in the volumes of the caudate/putamen, globus pallidus, substantia nigra, and hippocampus, and in the thickness of motor cortex (see Table 5). However, the volume of the subthalamic nucleus was found to be significantly reduced in heterozygous mice ($t = 7.256$; $df = 2$; $P = 0.018$). The numerical density of neurons (N_V) did not differ significantly in any of the regions examined. When the total number of neurons in a region was calculated from estimates of neuronal N_V and regional volume, there were significantly fewer neurons (approximately 45%) in the subthalamic nucleus of heterozygous mice ($t = 6.849$; $df = 2$; $P =$

Table 5. Morphometric Variables of Brains of Heterozygotes for the Hdh^{ex5} Mutation and Controls

Measurement	Control (n = 2)	Heterozygotes (n = 2)	P Value
Brain weight (mg)	400 ± 10	430 ± 10	NS
Caudate/putamen			
Volume (mm^3)	9.849 ± 0.333	8.988 ± 1.188	NS
N_v neurons	128,748 ± 11,703	140,555 ± 21,347	NS
Total neurons	1,217,788 ± 68,172	1,237,954 ± 24,882	NS
Neuron profiles (μm^2)	108 ± 1	100 ± 13	NS
Globus pallidus			
Volume (mm^2)	1.075152 ± 0.019443	0.817519 ± 0.127867	NS
N_v neurons	34,831 ± 2,845	26,994 ± 4,986	NS
Total neurons	37,504 ± 3,736	21,430 ± 625	NS
Neuron profiles (μm^2)	225 ± 1	178 ± 13	NS
Subthalamic nucleus			
Volume (mm^3)	0.132678 ± 0.005970	0.089158 ± 0.000573	0.01
N_v neurons	201,313 ± 2,532	170,719 ± 13,906	NS
Total neurons	26,725 ± 1,538	14,729 ± 838	0.02
Neuron profiles (μm^2)	118 ± 4	114 ± 19	NS
Substantia nigra			
Volume (mm^3), pars compacta	0.156043 ± 0.004276	0.136227 ± 0.015522	NS
Volume (mm^3), pars reticulata	0.414868 ± 0.030772	0.351587 ± 0.062205	NS
N_v neurons, pars reticulata	21,925 ± 2,635	21,272 ± 707	NS
Total neurons, pars reticulata	9,015 ± 419	7,435 ± 1,075	NS
Neuron profiles (μm^2)	209 ± 12	195 ± 11	NS
Hippocampus			
Volume (mm^3)	9.459 ± 0.489	10.005 ± 0.957	NS
Motor Cortex			
Thickness (μm^2)	1088 ± 51	1083 ± 118	NS

Values are given as means ± SEMs. NS, not significant.

0.021). In the globus pallidus, the mean value for total neuron number was 43% less in heterozygous mice compared with controls, but this difference was only of borderline significance (t = 4.243; df = 2; P = 0.051). The mean neuronal profile area was similar between the two groups in all the regions examined.

Discussion

Targeted Disruption of the *Hdh* Gene Results in Early Embryolethality

To explore the normal function of the HD gene and its role in development, we have disrupted the murine *Hdh* gene in exon 5 (Hdh^{ex5}). No liveborn mice (0 of 225) homozygous for Hdh^{ex5} were evident (Table 2; $p < 10^{-6}$). Because the liveborn progeny were derived from intercrosses of heterozygotes originating from three independently targeted ES cell lines, the lack of Hdh^{ex5} live offspring is not due to another mutation inadvertently generated in one ES cell line. These data clearly show that homozygosity for the Hdh^{ex5} mutation is lethal during embryonic development.

Analysis of 173 phenotypically normal embryos at different stages of gestation revealed that only four (2.37%) were homozygous mutants (Table 3; $p < 10^{-6}$). In contrast, genotyping of 35 resorbed embryos from 7.5 to 12.5 days gestation revealed that 28 (80%) were homozygous mutants (Table 4; $p < 10^{-6}$). The high frequency of postimplantation resorptions, lack of phenotypically normal-looking *Hdh* mutant (−/−) embryos after 8.5 days of gestation, and complete absence of liveborns homozygous for this mutation clearly show that the murine *Hdh* gene is essential for early postimplantation development.

Hdh^{ex5} mutants die at around E7.5 and display a phenotype in which gastrulation is significantly disturbed (Figure 4). During gastrulation in mammalian development, the three germ layers (ectoderm, mesoderm, and endoderm) are generated. While the precise cause of embryolethality is not yet determined, our results suggest that although the three germ layers are formed, subsequent failure to neurulate leads to complete disorganization of the embryo such that it never forms somites, nodes, or the notochord and does not proceed to organogenesis.

This indicates that mesoderm is formed, but that the normal *Hdh* protein may be critical for neurulation and development of the anterior–posterior axis. It is possible that inductive events between the chordamesoderm and surface ectoderm do not occur in the homozygous mutant embryos, leading to cessation of development. Clearly, the HD gene plays a crucial role in normal gastrulation.

Numerous other naturally occurring mutations and gene targeting experiments have also been shown to result in lethality during gastrulation due to primary disturbances in the primitive ectoderm (reviewed by Copp, 1995). These studies suggest that many of these genes, including the HD gene, may play crucial roles either as regulatory molecules underlying gastrulation in vertebrates or for essential cellular housekeeping functions that may be important for exchanging nutrients with the mother (Copp, 1995).

Behavioral Changes in Heterozygous Mice with the Hdh^{ex5} Mutation

Hdh^{ex5} mice differed from controls in several important ways, the most apparent being increased reactivity to handling. These mice were more active than controls when

placed in a novel photocell cage. This effect was seen in both light and dark conditions, in which crossings were more than two times greater in the heterozygous mice. Taken together, the motor activity data suggest that the *Hdh*^{ex5} mice habituate more slowly to the stimulus features of a novel environment and therefore remain more active than controls during both phases of the motor activity test. These changes in motor activity appear to be quite specific, as the *Hdh*^{ex5} mice performed normally on two spatial tasks (Figure 5).

T maze alternation, the 8-arm maze, and foraging for food assess the ability of a rodent to use memory of previous responses within a trial to plan subsequent responses and spatial function. Both groups of mice performed these maze tasks equally well, indicating normal short-term memory and spatial function.

The performance of *Hdh*^{ex5} mice on the Morris water maze task was particularly revealing. The hidden platform version of this task has been used to provide an unambiguous assessment of spatial abilities in rodents (Morris, 1981). When tested for the first time with the hidden platform in a fixed location, mutant mice performed as well as controls, with both groups showing normal learning curves and intact spatial memory on a memory probe trial (Figure 5). Therefore, it seems that *Hdh*^{ex5} mice have normal capacity for spatial navigation, memory for location in space, and normal short-term learning ability. Furthermore, they must have the normal perceptual and motor capacities required to see extramaze visual stimuli located in the test room and to exhibit normal swimming behavior.

Despite normal functioning on the preceding phase of spatial learning in the water maze, mutant mice were severely affected during the reversal trials (Figure 5). They failed to reach the same degree of proficiency in latency to reach the platform and showed no memory of the correct platform location during a memory probe trial in which the platform was removed from the pool. This may reflect a deficit in cognitive flexibility in which a previously successful strategy must be inhibited to develop a new strategy that is appropriate for a change in the demands of the task. Mutant mice appeared to be incapable of making this strategy switch. It is noteworthy that behavioral differences seen in *Hdh*^{ex5} mice relative to controls are similar to those seen in rodents with lesions to the basal ganglia. Deficits in switching from one set of learned responses to another is a well-documented behavioral correlate of damage to the basal ganglia and, in particular, to the dorsal striatum (Robbins and Everitt, 1992). Proactive interference by the original memory of the location of the platform may provide an alternative explanation of these data. Kainic acid lesions of the dorsal striatum that in part reproduce the neurochemical profile of HD can also cause an increase in spontaneous locomotor activity (Dunnet and Iverson, 1981). Rats with similar lesions performed normally in the initial acquisition of a water maze task, but when the platform was moved to another quadrant, lesioned animals were impaired relative to controls (McDonald and White, 1994), findings similar to those seen in *Hdh*^{ex5} mice.

Morphological Changes in the Brains of Mice Heterozygous for the *Hdh*^{ex5} Mutation

We have demonstrated significant decreases in both the volume of the subthalamic nucleus and the total number of subthalamic neurons in the two heterozygous mice compared with two littermate controls (Figure 6; Table 5). The total number of neurons in the globus pallidus appeared to be reduced, although morphometric analyses would be required on a larger subject sample to verify this observation. In contrast, no differences at all were seen in the caudate/putamen, substantia nigra, and hippocampus or in the thickness of the cerebral cortex. The 45% reduction in the number of subthalamic neurons in heterozygous mice could result from decreased neurogenesis during prenatal development or from increased apoptosis during late prenatal or early postnatal development. A third possibility is that subthalamic neuron loss is due to necrosis during early development, with rapid dissolution of necrotic tissue and no residual gliosis at 4 months of age. Alternatively, the influence of two genetic backgrounds on the growth of the subthalamic nucleus between heterozygotes and littermates has not been excluded.

The subthalamic nucleus, which is one of the five nuclei comprising the basal ganglia, functions in the extrapyramidal control of movement and has previously been implicated in the pathophysiology of HD (Folstein, 1989; Harper, 1991; Parent and Hazrati, 1995). Although neuronal loss from the subthalamic nucleus has been reported in HD (Lange et al., 1976), characteristic lesions involve a substantial loss of GABAergic medium-spiny neurons in the neostriatum (Lange et al., 1976; Graveland et al., 1985). In the early years of symptomatic HD, pathology in the neostriatum is minimal (Vonsattel et al., 1985), indicating that the pathophysiology of chorea precedes obvious necrosis in the basal ganglia. One question that arises is whether changes in the subthalamic nucleus might in some way be related to the striatal pathology and clinical phenotype of HD. It has previously been suggested that striatal lesions in HD alter the physiology of subthalamic neurons to produce chorea (Albin et al., 1989). Interestingly, acute lesions of the subthalamic nucleus due to stroke (Whittier, 1947) or induced experimentally in primates (Carpenter et al., 1950) manifest, with ballismus that is exaggerated, high amplitude chorea. In contrast, little is known concerning the effect of chronic, continued damage to the subthalamic nucleus.

Implications for the Pathogenesis of HD

The *Hdh*^{ex5} mutation in the murine HD gene results in embryolethality before E8.5, indicating that this gene is expressed very early in development and that there is no functional redundancy for this gene. In contrast, humans homozygous for the CAG mutation survive and have a phenotype (Wexler et al., 1987; Myers et al., 1989; Kremer et al., 1994) similar to heterozygotes for this mutation. Furthermore, there is no report of increased miscarriage rate in offspring of parents both heterozygous for the HD mutation. Taken together, these data provide compelling evidence that CAG expansion in the HD gene does not

result in complete loss of normal function of this gene. Furthermore, our data showing lethality of the mutant allele also argue against a complete dominant negative mechanism for the pathogenesis of HD in which the mutant gene results in complete loss of its own function and also inactivates the normal product. In contrast, the findings of embryolethality for mice homozygous for the mutation and equivalence of the homozygote and heterozygote phenotype of HD in humans are more compatible with CAG expansion, conferring a novel gain of function independent of the normal physiological role of the protein. Recent evidence clearly shows that the CAG repeat in the HD gene is indeed translated into a polyglutamine stretch (Jou and Myers, 1995; Sharp et al., 1995).

Mice heterozygous for the *Hdh*^{ex5} mutation have behavioral deficits similar to that seen in rodents with lesions in the striatum, and two of these same mice analyzed have significant reductions of neurons in the subthalamic nucleus. Intriguingly, this nucleus also shows obvious neuronal loss (25%) in patients with HD (Lange et al., 1976), which raises the question whether partial loss of normal function of this gene could result in neuronal loss in the basal ganglia. An alternative possibility is that expression of the truncated HD protein in the heterozygous mice results in a phenotype with some similarity to HD not due to partial loss of function, but due to the truncated protein acting as a toxic product.

Interestingly, CAG expansion in the androgen receptor gene is associated with X-linked spinal and bulbar muscular atrophy (La Spada et al., 1991), but affected males also have signs of partial loss of normal androgen receptor function, manifested with gynecomastia and reduced fertility (Arbizu et al., 1983). While CAG amplification in the androgen receptor gene confers novel functional properties (Mahtre et al., 1993), this is associated at the same time with partial loss of normal function. Pathological involvement of the basal ganglia in mice heterozygous for the *Hdh*^{ex5} mutation suggests that partial loss of normal function of the HD gene might also contribute to the phenotype of HD.

Data presented here suggest that the HD gene plays an essential function during gastrulation in early embryogenesis and that it may also have an important physiological role in the basal ganglia. Similar to the androgen receptor gene, it is possible that CAG expansion in the HD gene also results in partial loss of physiological function of this gene, with subsequent mild deficits in this region of the brain. Partial loss of normal function, however, would be insufficient to result in a clinical phenotype. For example, one patient with a balanced translocation that disrupted the HD gene between exons 41 and 42 was still asymptomatic at age 46. In this patient, however, the protein contains nearly two thirds of the normal product, which may be sufficient to exert its normal physiological role (Ambrose et al., 1994).

We therefore propose a model for the pathogenesis of HD that involves a gain of novel properties, in addition to a partial loss of its normal physiological role. Selective neuronal death caused by dysfunction of this widely expressed gene could reflect restricted expression of a protein that has altered interaction with an HD gene product with an expanded polyglutamine stretch. In addition, partial loss of the physiological role of this gene in the basal ganglia could also contribute to the HD phenotype.

This model could have important implications for the design of therapeutic strategies as well as novel research directions. One approach to treatment of HD is to decrease the expression of the HD gene, and this might be expected to mitigate the phenotype. An alternate approach may be to determine which cellular proteins specifically interact with the HD gene product and to direct attention to interference with this interaction. This approach could also be insufficient to cure HD, as additional strategies to replace the partial loss of normal function of the HD gene may be necessary to reach that goal.

Experimental Procedures

Constructing the pHdhNeo6 Targeting Vector

A phage genomic library from the 129/Sv mouse strain (Stratagene) was screened using a probe encompassing exon 5 of the murine *Hdh* cDNA (Lin et al., 1994). A 5.4 kb genomic fragment including murine exons 4 and 5 was subcloned into pBluescriptII KS(+) (Stratagene). A 3.5 kb EcoRI–XbaI clone was derived by digestion with EspI to remove a 600 bp fragment encompassing intron 4 and approximately half of exon 5 (see Figure 1A). The EspI site was end-filled with Klenow (Sambrook et al., 1989), and a blunt-ended EcoRI–XhoI fragment from *PGKneobpA* (Soriano et al., 1991) was introduced.

Detecting Homologous Recombination in ES Cells

PCR was used to screen for homologous recombination using primers *P6* (GGAGGCTAGAATGCTTGCAG) and *P7* (TCTATGGCTTCTGAGGCGGA). Following an initial denaturation step (96°C for 1 min), 40 cycles of PCR were performed (94°C for 1 min, 60°C for 90 s, 72°C for 120 s) with a final step of 72°C for 10 min, using the 9600 Perkin–Elmer machine.

Generation of Germline Chimeras

Blastocysts were collected from pregnant C57BL/6J females at 3.5 days postcoitum. Approximately 8–10 ES cells were microinjected and implanted into pseudopregnant ICR foster mothers. Chimeras identified by the presence of an agouti coat color were test-mated with C57BL/6J females. Agouti offspring were tested for the targeted *Hdh* gene by Southern blotting.

RT-PCR and Sequencing

Total mRNA was extracted from freshly isolated tissue using the guanidium isothiocynanate method (Chomczynski and Sacchi, 1987). Poly(A)$^+$ RNA was extracted using the Micro-Fast Track mRNA isolation kit (Invitrogen Corporation). RT was performed using the SuperScript preamplification system (GIBCO BRL) with both a gene-specific primer (*P16*) (AATTTCATTGTCATTTGCGA) and random hexamers in separate reactions. The RT product (5 μl) was used for PCR amplification using primers *P11* (CGATGCGGAGTCAGATGTCA) and *P14* (GGTCTTTTGCTTGTTCGGGT). The shorter 167 bp PCR product was subcloned using the TA cloning kit (Invitrogen Corporation) and sequenced using an Applied Biosystems automated sequencer.

Genotype Analysis

For PCR analysis, embryos were incubated overnight in a lysis buffer containing 20 mM Tris, 50 mM KCl, 0.45% NP-40, 0.45% Tween-20, 0.01% gelatin, and 100 μg/ml proteinase K and overlaid with mineral oil. The samples were then incubated at 94°C for 10 min, and 5 μl was used for a 25 μl PCR in the 9600 Perkin–Elmer machine. Genotyping was carried out using *P8* (TGGCAAGACAATAGCAGGCA), a *neo*-specific primer; *P586* (AGTTTGCGTGCTGCCCTGTG), a primer derived from exon 5 of mouse; and *P9* (CCAGACAGGACATAGCTAGG), a primer from intron 5 (Figure 1). All three primers (*P8*, *P9*, and *P586*) were used together in a single PCR.

Histology

Embryos and whole decidua were fixed in Bouin's solution and embedded in paraffin wax. Serial sections of 5 μm were prepared and stained with hematoxylin and eosin.

Behavior Studies

Locomotion Test

Spontaneous locomotion was assessed using three clear Plexiglas photocell cages (25 cm × 25 cm × 26 cm) placed individually inside large dark chambers (45 cm × 45 cm × 100 cm). Individual photocell cages were illuminated by a 70 mW light bulb and had four parallel infrared photocell beams (two on each axis) located 2 cm above the floor and 8 cm from each corner of the cage. Interruptions of any beam were registered incrementally by a microcomputer and were summed in 10 min bins during the locomotion test. Mice were placed individually in the apparatus, and spontaneous locomotion was assessed for a 4 hr trial. For the first 2 hr, the house lights were left on (light phase), and for the final 2 hr the lights were off (dark phase). Mice were tested in the middle of their light cycles, between 1 p.m. and 5 p.m.

T Maze Alternation Test

Following the locomotion test, mice were housed individually and were deprived of food over 7 days to 85%–90% of their free-feeding weight. Mice were then tested for reinforced alternation responses on a T maze. The T maze was made of clear Plexiglass and consisted of a two goal arms (20 cm × 10 cm × 12 cm), each with a small plastic food cup (3 cm diameter and 0.5 cm deep) at the distal end, and a start arm (36 cm × 10 cm × 12 cm), which could be blocked off by a wooden barrier (10 cm × 18 cm). On the first 2 days, each animal was habituated to the T maze for a 10 min period, during which pieces of Kellogg's Froot Loops cereal were distributed on the T maze. Animals were subsequently tested on a standard alternation paradigm for 3 days. The first trial was a forced choice in which mice could enter only one baited goal arm, chosen at random. After entering the open arm, the mouse was confined there until food was consumed, following which the mouse was placed back in the start arm and confined for 15 s. In 12 subsequent trials per day, we required the animals to choose the opposite arm from the one visited on the previous trial to receive food reinforcement. Following a correct choice, the mouse was again confined to the goal arm until it had eaten the food. An incorrect choice resulted in confinement in that arm for 30 s, after which the mouse was placed in the start arm to await the next trial. The number of correct choices and the latency to reach the food cup of the chosen arm were recorded.

Radial-Arm Maze Test

At 1 week after the completion of the T maze alternation tests, mice were given 7 days of testing on a radial-arm maze task. The maze was constructed from plywood and consisted of a central octagonal platform (35 cm diameter) with eight arms radiating from the platform (35 cm × 9 cm) with a plastic food cup at the distal end of each arm. On day 1 of training, food was distributed around the center of the platform and in the food cups of four randomly selected arms. Individual mice were placed in the center of the maze and permitted to forage until all four pieces of food had been eaten from the food cups and all eight arms had been visited or until 10 min had elapsed. For all subsequent daily trials, pellets were placed in the food cups of four arms selected at random. A novel set of four arms was chosen each day, and optimal foraging behavior required animals to minimize reentries into arms visited previously within a daily trial. Errors were scored as revisits to any arm entered previously. The experimenter recorded arm choices and latencies to reach the food cup in the first arm chosen and the total time required to complete the daily trial.

Morris Water Maze Task

After completion of the radial-arm maze test, mice were provided with food ad libitum and 1 week later were tested on the standard Morris water maze (Morris, 1981) paradigm. The water maze was a large white plastic tank 180 cm in diameter and 54 cm in height. The pool was filled with 20 cm of water at room temperature (22°C), rendered opaque by adding one can of white powder paint. The submerged invisible escape platform was 19 cm in diameter. On top of the platform was a piece of metal mesh measuring 15 cm × 15 cm. The testing room had ample spatial cues taped to the walls. Swimming behavior was recorded by a video camera mounted on the ceiling across the pool that measured the path length and the time taken by each mouse to find the hidden platform for each trial.

Spatial abilities were assessed in four distinct phases. In the first phase, mice were given four to six trials per day (16 trials in total), with an intertrial interval of 4–5 min. At the start of each trial, the mouse was placed in the pool at one of four release points (north, south, east, or west), and it swam until it found the hidden platform located in the center of the northwest quadrant or until 120 s had elapsed. Failure to locate the submerged platform in the allotted time resulted in the mouse being placed on the platform for 15 s, after which it was returned to its home cage. The release point order was randomized. When the mice demonstrated symtotic performance during the four trials on day 3, the mice were given a 60 s memory probe trial with the platform removed from the pool. In the second phase, the amount of time spent in each quadrant of the pool was calculated along with the number of crossings over the platform site. The third phase (days 4 and 5, consisting of six and four trials, respectively) tested mutant mice for reverse spatial strategy by swimming directly to the platform, repositioned in the southeast location. In the fourth phase, a second memory probe trial was performed in which the platform was again removed from the pool and the percentage of time spent in each quadrant was measured, along with the number of crossings over the platform site.

Data Analysis

Statistical analyses employed 2-factor between/within design analysis of variance (ANOVA) and 1-factor ANOVA for simple main effects. For the probe trials of the water maze experiment, Tukey's post hoc tests were used to determine in which quadrants of the pool animals spent significantly more time. All values reported in the text and figures are expressed as means ± SEMs.

Histology and Morphometry of Brains of Mice Heterozygous for the *Hdh*^{ex5} Mutation

Brains from two heterozygous mice and two wild-type controls were examined at 4 months of age. Mice were anesthetized by an intraperitoneal injection of sodium pentobarbital (80 mg/kg) and perfused through the ascending aorta with a fixative solution containing 4% paraformaldehyde and 1% glutaraldehyde in 0.1 M phosphate buffer (pH 7.4) at a perfusion pressure of 120 mm/Hg^0 for 60 min. The brains were removed, weighed, and placed in additional fixative solution for 24 hr. The brains were bisected in the midline, and serial frozen sections were cut at 30 μm in the transverse plane throughout the entire length of the right half of each brain. Every second section in this series was mounted on chrome alum gelatin–coated slides and stained for Nissl substance using 0.1% thionin in 0.1 M acetate buffer (pH 3.7).

All histological sections were coded to prevent experimenter bias during the morphometric analyses. The individual volumes of the caudate/putamen, globus pallidus, subthalamic nucleus, substantia nigra (i.e., both the pars compacta and the pars reticulata), and hippocampus were measured on the serial Nissl sections in millimeters cubed. Individual sections were visualized at a final magnification of 48×, and the area of each nucleus was measured in square millimeters using an image analysis system (Bioquant System IV, RandM Biometrics). The volume was calculated from

$$V = \Sigma_A \times T \times 2,$$

where Σ_A is the sum of area measurements, T is section thickness, and 2 is the periodicity of the section sample.

Measurements of the numerical density of neurons (N_V; neurons per millimeter cubed) were made in the caudate/putamen, globus pallidus, subthalamic nucleus, and substantia nigra using the methodology of Abercrombie (1946). In brief, sections were examined at a final magnification of 1025×. Neurons were counted when their nuclear profiles contained a distinct nucleolus. The N_V was calculated from

$$N_V = N_A/(D + T),$$

where N_A is the number of neurons per unit area of section, D is the mean diameter of the nucleolus, and T is section thickness. The total number of neurons for each nucleus was calculated using estimates of N_V and volume. For individual neurons, the profile areas of the cell

body were measured in the plane of focus that contained the nucleolus from 100 randomly selected neurons in each nucleus. The statistical significance of direct comparisons between heterozygous mice and wild-type controls was determined using the Student's t test.

Acknowledgments

Correspondence should be addressed to M. R. H. We thank our colleagues in our laboratories for their useful comments and support. In particular, we want to acknowledge Martina Metzler, Rona Graham, Natalie Spence, Michael Iagallo, David Kozuki, Rob Campbell, Lynn Raymond, Daniel Phaneuf, and Phil Soriano. We thank Chris Ross for the generous gift of antibody AP78 to the HD protein. This study was supported by the National Centre of Excellence (Genetics) and the Medical Research Council (MRC) (Canada). M. R. H. is an established investigator of the British Columbia Children's Hospital. J. N. has been supported by a Bluma Tischler Fellowship and is now an MRC (Canada) postdoctoral fellow.

Received April 24, 1995; revised May 5, 1995.

References

Abercrombie, M. (1946). Estimation of nuclear population from microtome sections. Anat. Rec. *94*, 239–247.

Albin, R. L., Young, A. B., and Penney, J. B. (1989). The functional anatomy of basal ganglia disorders. Trends Neurosci. *12*, 366–375.

Ambrose, C. M., Duyao, M. P., Barnes, G., Bates, G. P., Lin, C. S., Srinidhi, J., Baxendale, S., Hummerich, H., Lehrach, H., Altherr, M., Wasmuth, J., Buckler, J., Church, D., Housman, D., Berks, M., Micklem, G., Durbin, R., Dodge, A., Read, A., Gusella, J., and MacDonald, M. E. (1994). Structure and expression of the Huntington's disease gene: evidence against simple inactivation due to an expanded CAG repeat. Somat. Cell Mol. Genet. *20*, 27–38.

Arbizu, T., Santamaria, J., Gomez, J. M., Quilez, A., and Serra, J. P. (1983). A family with adult spinal and bulbar muscular atrophy, X-linked inheritance and associated testicular failure. J. Neurol. Sci. *59*, 371–382.

Carpenter, M. B., Whittier, J. R., and Mettler, F. A. (1950). Analysis of choreoid hyperkinesia in the rhesus monkey: surgical and pharmalogical analysis of hyperkinesia resulting from lesions in the subthalamic nucleus of Luys. J. Comp. Neurol. *92*, 293–331.

Chomczynski, P., and Sacchi, N. (1987). Single-step method of RNA isolation by acid guanidinium thiocyanate–phenol–chloroform extraction. Anal. Biochem. *162*, 156–159.

Copp, A. J. (1995). Death before birth: clues from gene knockouts and mutations. Trends Genet. *11*, 87–93.

Dunnet, S. B., and Iverson, S. D. (1981). Learning impairments following selective kainic acid–induced lesions within the neostriatum of rats. Behav. Brain Res. *2*, 189–209.

Folstein, S. E. (1989). Huntington's Disease: A Disorder of Families (Baltimore: Johns Hopkins University Press).

Graveland, G. A., Williams, R. S., and DiFiglia, M. (1985). Evidence for degenerative and regenerative changes in neostriatal spiny neurons in Huntington's disease. Science *227*, 770–773.

Harper, P. S. (1991). Huntington's Disease (London: W. B. Saunders).

Hayden, M. R. (1981). Huntington's Chorea (London: Springer-Verlag).

Hogan, B., Constantini, F., and Lacy, E. (1986). Manipulating the Mouse Embryo: A Laboratory Manual (Cold Spring Harbor, New York: Cold Spring Harbor Laboratory Press).

Huntington's Disease Collaborative Research Group (1993). A novel gene containing a trinucleotide repeat that is expanded and unstable on Huntington's disease chromosomes. Cell *72*, 971–983.

Jou, Y.-S., and Myers, R. M. (1995). Evidence from antibody studies that the CAG repeat in the Huntington disease gene is expressed in the protein. Hum. Mol. Gen. *4*, 465–469.

Kremer, H. P. H., Goldberg, Y. P., Andrew, S. E., Squitieri, F., Theilmann, J., Telenius, H., Zeisler, J., Lin, B., Adam, S., Benjamin, C., Hayden, M. R., and the International Huntington's Disease Research Group (1994). Worldwide study of the Huntington's disease mutation: the sensitivity and specificity of repeated CAG sequences. N. Engl. J. Med. *330*, 1401–1406.

Lange, H., Thorner, G., Hopf, A. V., and Schroder, K. F. (1976). Morphometric studies of the neuropathological process in choreatic diseases. J. Neurol. Sci. *28*, 401–425.

La Spada, A. R., Wilson, E. M., Lubahn, D. B., Harding, A. E., and Fischbeck, K. H. (1991). Androgen receptor gene mutations in X-linked spinal and bulbar muscular atrophy. Nature *352*, 77–79.

Li, S. H., Schilling, G., Young, W. S., III, Li, X. J., Margolis, R. L., Stine, O. C., Wagster, M. V., Abbott, M. H., Franz, M. L., Ranen, N. G., et al. (1993). Huntington's disease gene (*IT15*) is widely expressed in human and rat tissues. Neuron *11*, 985–993.

Lin, B., Rommens, J. M., Graham, R. K., Kalchman, M. A., McDonald, H., Nasir, J., Delaney, A., Goldberg, Y. P., and Hayden, M. R. (1993). Differential 3′ polyadenylation of the Huntington disease gene results in two mRNA species with variable tissue expression. Hum. Mol. Genet. *2*, 1541–1545.

Lin, B., Nasir, J., MacDonald, H., Hutchinson, G. B., Graham, R. K., Rommens, J. M., and Hayden, M. R. (1994). Sequence of the murine Huntington disease gene: evidence for conservation, alternate splicing and polymorphism in a triplet (CCG) repeat. Hum. Mol. Genet. *3*, 85–92.

Lin, B., Nasir, J., Kalchman, M. A., McDonald, H., Zeisler, J., Goldberg, Y. P., and Hayden, M. R. (1995). Structural analysis of the 5′ region of mouse and human Huntington disease genes reveals conservation of putative promoter region and di- and trinucleotide polymorphisms. Genomics *25*, 707–715.

Mahtre, A. N., Trifiro, M. A., Kaufman, M., Kazemi-Esfarjani, P., Figlewicz, D., Rouleau, G., and Pinsky, L. (1993). Reduced transcriptional regulatory competence of the androgen receptor in X-linked spinal and bulbar muscular atrophy. Nature Genet. *5*, 184–188.

McDonald, R. J., and White, N. M. (1994). Parallel information processing in the water maze: evidence for independent memory systems involving dorsal striatum and hippocampus. Behav. Neural Biol. *61*, 260–270.

Morris, R. G. M. (1981). Spatial localization does not require the presence of local cues. Learn. Motiv. *12*, 239–260.

Myers, R. H., Leavitt, J., Karner, L. A., Farrer, L., Jagedeesh, J., McFarlane, H., Mastromouro, C. A., Mark, R. J., and Gusella, J. F. (1989). Homozygote for Huntington disease. Am. J. Hum. Genet. *45*, 615–618.

Nasir, J., Lin, B.-Y., Bucan, M., Nadeau, J., and Hayden, M. R. (1994). The murine homologue of the Huntington disease gene (*Hdh*) maps to mouse chromosome 5 within a region of conserved synteny with human chromosome 4p16.3. Genomics *22*, 198–201.

Parent, A., and Hazrati, L. (1995). Functional anatomy of the basal ganglia. II. The place of subthalamic nucleus and external pallidum in basal ganglia circuitry. Brain Res. Rev. *20*, 128–154.

Robbins, T. W., and Everitt, B. J. (1992). Functions of dopamine in the dorsal and ventral striatum semin. Neuroscience *4*, 119–127.

Sambrook, J., Fritsch, E. F., and Maniatis, T. (1989). Molecular Cloning: A Laboratory Manual, Second Edition (Cold Spring Harbor, New York: Cold Spring Harbor Laboratory Press).

Sharp, A. H., Loev, S. J., Schilling, G., Li, S.-H., Li, X.-J., Bao, J., Wagster, M. V., Kotzuk, J. A., Steiner, J. P., Lo, A., Hedreen, J., Sisodia, S., Snyder, S. H., Dawson, T. M., Ryugo, D. K., and Ross, C. A. (1995). Widespread expression of Huntington's disease gene (IT15) protein product. Neuron *14*, 1065–1074.

Soriano, P., Montgomery, C., and Bradley, A. (1991). Targeted disruption of the *c-src* proto-oncogene leads to osteopetrosis in mice. Cell *64*, 693–702.

Strong, T. V., Tagel, D. A., Vades, J. M., Elmer, L. W., Boehm, K., Swaroop, M., Kaatz, K. W., Collings, F. S., and Albin, R. L. (1993). Widespread expression of the human and rat Huntington's disease gene in brain and nonneural tissues. Nature Genet. *5*, 259–265.

Vonsattel, J.-P., Myers, R. H., Stevens, T. J., Ferrante, R. J., Bird, E. D., and Richardson, E. P., Jr. (1985). Neuropathological classification of Huntington's disease. J. Neuropath. Exp. Neurol. *44*, 559–577.

Wexler, N. S., Young, A. B., Tanzi, R. E., Travers, H., Starosta-Rubenstein, S., Penney, J. B., Snodgrass, S. R., Shoulson, I., Gomez, F., Ramos-Arroyo, M. A., Penchaszadeh, G., Moreno, R., Gibbons, K., Faryniarz, A., Hobbs, W., Anderson, M. A., Bonilla, E., Conneally, P. M., and Gusella, J. F. (1987). Homozygotes for Huntington disease. Nature *326*, 194–197.

Whittier, J. R. (1947). Ballism and the subthalamic nucleus (nucleus hypothalamus corpus Luysi). Arch. Neurol. Psych. *58*, 672–692.

Willems, P. J. (1994). Dynamic mutations hit double figures. Nature Genet. *8*, 213–215.

Note Added in Proof

The present address of J. D. M. is Howard Hughes Medical Institute, Division of Cellular and Molecular Medicine, University of California, San Diego, La Jolla, California 92093.